Chinese Astronomy and Astrophysics 45 (2021) 147–161

CHINESE
ASTRONOMY
AND ASTROPHYSICS

Statistical Investigation on Galactic Cosmic Rays and Solar Wind Variation Based on ACE Observations† ⋆

GUO Xiao-cheng[1,2△] JIANG Wence[1,2] LI Hui[1,2]

[1] *State Key Laboratory of Space Weather, National Space Science Center, Chinese Academy of Sciences, Beijing 100190*

[2] *College of Earth and Planetary Sciences, University of Chinese Academy of Sciences, Beijing 100049*

Abstract Based on the Galactic Cosmic Rays (GCRs) and plasma observations from ACE spacecraft, the relation between GCR counts and solar wind parameters during the two periods of solar minimums (the years of 2007.0-2009.0 and 2016.5-2019.0) was analyzed by means of the Superposed Epoch Analysis (SEA) method. The results indicate that GCRs are strongly modulated by Corotating Interaction Regions (CIRs) in solar wind, the Stream Interfaces (SIs) sandwiched between fast and slow solar wind are closely related with the depression of GCR counts. The mechanism of the GCR variation was investigated through the empirical diffusion coefficients. The so-called "snow-plough" effect of GCR variation prior to the SI crossing appears during the first period, then the GCR counts decrease after the crossing, which corresponds to the sudden drop of diffusion coefficient at the SI. However, this effect is not observed for the second period, the decrease of GCR counts may be caused by the enhancement of the diffusion coefficient after the SI crossing. Moreover, Heliospheric Current Sheet (HCS) correlates with GCR counts well, the GCRs drift along the current sheet, and then accumulate to a pileup structure. The interplay between drift and diffusion determines the GCR distribution and variation at a heliocentric distance of 1 AU.

† Supported by the Strategic Priority Research Program of Chinese Academy of Sciences Grant Nos. XDB 41000000, XDA15052500, XDA17010301, QYZDJ-SSW-JSC028, NNSFC Grant Nos. 41874171, 41674146, and 41731070, in part by the Specialized Research Fund for State Key Laboratories of China and NSSC research fund for key development directions, and the Civil Aerospace "13th Five-Year Plan" Preliminary Research in space science (project Nos. D020301, D030202).

Received 2020–01–14; revised version 2020–09–25

⋆ A translation of *Chin. J. Space Sci.* Vol. 40, No. 6, pp. 969–979, 2020

△ xcguo@swl.ac.cn

doi: 10.1016/j.chinastron.2021.05.002

Key words galactic cosmic rays—co-rotating interaction regions—stream interface—heliospheric current sheet

1. INTRODUCTION

Galactic cosmic rays (GCRs) are the high energy charged particles (mainly protons) from the outside heliosphere, and are generally thought to be accelerated by shocks associated with supernova explosions[1], with an energy range above 100 MeV$\cdot$nuc^{-1}. Voyager 1 has been measuring the nearly constant GCR flux since the heliopause crossing in august of 2012[2], which confirmed the theoretical expectation that heliopause is the modulation boundary for GCRs[3]. After entering the heliosphere, most of GCRs are modulated by the heliospheric magnetic field, for example, the GCRs with rigidity less than 10 GV are scattered in the inner heliosphere because of their smaller gyro-radius than the scale of typical solar wind structure[4]. Meanwhile, the GCRs are scattered by the intrinsic magnetic irregularities (turbulence) which is imposed upon the outward expanding solar wind, and are swept away from the Sun. As a result, the GCR flux decreases along the inward radial direction from the heliopause[5]. Gradient and curvature drifts are the important mechanisms that assist the global transport of GCRs in the heliosphere[6]. From a global view, GCRs drift along the heliospheric current sheet (HCS) at low latitude, and escape at high latitude for the period of $qA < 0$, where q is the particle charge, and A is the polarity of the radial component of heliospheric magnetic field (HMF) in northern heliosphere. This drift pattern inverses for $qA > 0$. The observation has indicated that the polarity of HMF changes every 22 years, and the solar activity has a period of 11 years, and they affect the drift and diffusion of GCRs in the heliosphere, respectively, and result in the long-term variation of GCRs[7,8]. In the inner heliosphere, the 27 days solar rotation causes the short-term variation of solar wind, and GCR counts as well[9]. Some observations indicated that the long-term GCR variations may be produced by an accumulation of a large number of short-term transient events in the outer heliosphere[10,11]. Moreover, GCRs gain or lose energy when they travel through compression and rarefaction, respectively, for instance, at the termination shock or co-rotating interaction regions (CIRs)[7,12].

CIRs are formed by the overtaking of fast solar wind stream over the slow solar wind stream ahead, and co-rotate with the Sun[13]. They are commonly seen at the inner heliosphere ($\sim$ 1 AU from the Sun)[14]. CIRs may affect the short-term variation of GCRs because theoretically the particles may respond to changes in the solar wind speed (affecting GCR convection and energy changes), magnetic irregularities (diffusive effects), and the magnetic field magnitude (variations of drifts and diffusion). However, the main control factor is still in debate[15]. The observation showed that the solar wind speed in CIRs is well correlated with GCRs, showing the importance of GCR convection effect[16]. Specifically, the stream interfaces (SIs) between fast and slow solar wind streams and the leading edge (fast wave or shock) in CIRs always correspond to the depression of GCR intensities, it seems that the magnetic field and HCS do not organize the variation of GCRs[17]. The previous simulation showed that the GCR diffusion near SIs is much larger than the drift effect which is associated with a HCS crossing during the time of solar minimum[18]. Based on superimposed epoch analysis (SEA) on CIRs, a theoretical calculation showed that perpendicular diffusion coefficient for GCRs highly correlates with the GCR intensities at a heliocentric distance of 1 AU, indicating the key role of diffusion effects for GCR transport[19]. However, some observations showed that GCR variations are associated with the HCS crossings in CIRs[20,21]. For the HCS crossings in strong-compression of solar wind (such as CIRs), a peak in neutron counts was observed preceding the HCS crossing, followed by a large drop after the crossing. For weak-compression HCS crossings, the neutron counts have a tendency to peak in the away magnetic field sector[22]. The enhancement of GCR flux before the drop is attributable to the so-called 'snow-plough' effect, which is commonly considered to be associated with the GCR scattering by CIRs as a barrier effect[14]. The ground observation of GCRs from global muon detector network also supported the important role of drift effects on the GCR intensities[23]. The above statement showed the disagreement on the physical mechanism of GCR variation in the inner heliosphere. It is necessary to investigate this topic based on more observations. In this paper, we will analyze and discuss the physical relation between solar wind and GCR counts based on ACE observations.

2. DATA AND METHODS

ACE (Advanced Composition Explorer) is a spacecraft orbiting at Lagrangian point (L1) more than 30 years since its launching in August of 1997[24]. Here we used the level 2 data with 1 hour resolution from the three equipment on ACE, namely the solar wind density, bulk speed, and temperature from the Solar Wind Electron Proton Alpha Monitor (SWEPAM), magnetic field from the Magnetometer (MAG), and cosmic rays from the Cosmic Ray Isotope Spectrometer (CRIS). Instead of the long-term variation of GCR due to the periodic solar activities, the short-term variation will be investigated in this work based on the observation. Two time intervals were selected for the data analysis, the first one from the year 2007.0 to 2009.0, and the second from 2016.5 to 2019.0, roughly correspond to the solar minimum at the begin and end of the 24th solar cycle, respectively. During the solar minimum, although some fast wind streams originate from the coronal holes at low and middle latitudes[25], most of them come from the solar surface at high latitudes, and the slow streams at low latitudes[26]. The eruptive solar wind events, e.g., interplanetary coronal mass ejections (ICMEs) are less frequently observed during the periods, and most solar wind events are expected to be CIRs.

The stream interfaces (SIs) are distinguished by the following criteria[27]: the sudden increase of solar wind speed, the maximum of total pressure (thermal plus magnetic pressures). Simultaneously, the proton density is highly compressed and the temperature increase during SI crossing. Table 1 lists the crossing time of SIs during the two intervals, consisting of 82 and 94 events, respectively. The events during the first interval is same as those in the previous literature[28]. The HCS or magnetic sector boundaries are identified by the abrupt change of magnetic longitude under the RTN coordinate[29]. As Table 2 lists the time information of HCS, there are 79 events for the first interval, and 114 events for the second. For an individual HCS crossing, it is difficult to estimate the effect on GCR variation if the time of HCS event is too close to that of an SI. To exclude this situation, we simply remove the HCS events that occur within one day of an adjacent SI, and those within two days of an adjacent HCS. The filtered HCS events are shown as in Table 3, with 37 and 49 events for the two intervals, respectively, which can be used to analyze the effect of an individual HCS on the GCRs more accurately.

Table 1 Crossing time of the SIs in CIRs

2007.0029	2007.0280	2007.0400	2007.0780	2007.1007	2007.1173	2007.1584	2007.1766	2007.1932
2007.2274	2007.2466	2007.2684	2007.2915	2007.3070	2007.3198	2007.3466	2007.3768	2007.4165
2007.4505	2007.4695	2007.4925	2007.5043	2007.5234	2007.5493	2007.5661	2007.5729	2007.5971
2007.6070	2007.6190	2007.6517	2007.6686	2007.6820	2007.7035	2007.7193	2007.7388	2007.7539
2007.7788	2007.7968	2007.8153	2007.8270	2007.8567	2007.8660	2007.9419	2007.9595	2007.9882
2008.0117	2008.0345	2008.0662	2008.0840	2008.1099	2008.1596	2008.1869	2008.2333	2008.2589
2008.2909	2008.3094	2008.3375	2008.3853	2008.4048	2008.4328	2008.4532	2008.4828	2008.5092
2008.5274	2008.5554	2008.6045	2008.6296	2008.6728	2008.7046	2008.7502	2008.7768	2008.8002
2008.8174	2008.8246	2008.8511	2008.8739	2008.8998	2008.9221	2008.9290	2008.9430	2008.9745
2008.9974	2016.5027	2016.5163	2016.5495	2016.5738	2016.5878	2016.6048	2016.6453	2016.6689
2016.7188	2016.7402	2016.7905	2016.8157	2016.8640	2016.8994	2016.9347	2016.9714	2016.9985
2017.0476	2017.0704	2017.0833	2017.1296	2017.1478	2017.1636	2017.2179	2017.2341	2017.2670
2017.3032	2017.3692	2017.3817	2017.4021	2017.4215	2017.4426	2017.4557	2017.4829	2017.4983
2017.5194	2017.5380	2017.5517	2017.5900	2017.6108	2017.6257	2017.6639	2017.7031	2017.7385
2017.7776	2017.8130	2017.8510	2017.8881	2017.9056	2017.9267	2017.9438	2017.9604	2017.9798
2018.0001	2018.0212	2018.0355	2018.0564	2018.0689	2018.0849	2018.0952	2018.1272	2018.1462
2018.1578	2018.1994	2018.2095	2018.2215	2018.2711	2018.3000	2018.3417	2018.3734	2018.3894
2018.4128	2018.4616	2018.4753	2018.4833	2018.5094	2018.5524	2018.5596	2018.6210	2018.6336
2018.6505	2018.6824	2018.6930	2018.7244	2018.7661	2018.7826	2018.8047	2018.8441	2018.8583
2018.9055	2018.9329	2018.9680	2018.9897	2019.0114				

CRIS instrument provides the GCR flux or counts for the heavy ions with elements from $Z \simeq 2$ to 30, and energy intervals from ~ 50 to ~ 500 MeV·nuc^{-1}[24]. Although it was reported that the proton was measured as well[19], here we focus on heavy ions that can be obtained from the public database (*http://www.srl.caltech.edu/ACE/ASC/*). The heavy ions have the small abundance of $\sim 1\%$ among the total GCR particles, the counts of the elements from Z = 5 to 13 are accumulated together to represent the total GCR counts evaluated in this work. Figure 1 shows the temporal variation of solar wind and GCRs from the year 2008.5 to 2008.6, including the magnetic longitude in RTN coordinate, total pressure, bulk speed of solar wind, and GCR counts. The green dashed lines mark the HCS crossings, the red dashed lines are the crossings of SIs. In the fourth panel, the GCR counts are smoothed over 0.5 days and 30 days, shown as the black and blue curves, respectively. The former represents the short-term variation of the counts, and the latter indicates the variation at a much longer time-scale. The three SI crossings are associated with the depression of GCR counts from the black curve. For the three HCS crossings, GCRs seem to be accumulated near HCS for the first two events. The different behaviors of GCR counts for SI and HCS crossings indicate the existence of different physical mechanisms which will be explored in this work.

Table 2 Crossing time of all the HCS

2007.0015	2007.0220	2007.0392	2007.0701	2007.0774	2007.0972	2007.1164	2007.1433	2007.1536
2007.1699	2007.1929	2007.2189	2007.2270	2007.2462	2007.2684	2007.2909	2007.3044	2007.3169
2007.3462	2007.3717	2007.3793	2007.3911	2007.4158	2007.4328	2007.4485	2007.4692	2007.4901
2007.5024	2007.5248	2007.5453	2007.5660	2007.5725	2007.5947	2007.6191	2007.6652	2007.7010
2007.7418	2007.7758	2007.8175	2007.8530	2007.8862	2007.9249	2007.9594	2007.9822	2007.9864
2007.9957	2007.9991	2008.0106	2008.0309	2008.0835	2008.1094	2008.1575	2008.1827	2008.2316
2008.2543	2008.3075	2008.3298	2008.3807	2008.4069	2008.4327	2008.4434	2008.4520	2008.4822
2008.5067	2008.5521	2008.5773	2008.6256	2008.6481	2008.7024	2008.7240	2008.7740	2008.7945
2008.8513	2008.8736	2008.9230	2008.9427	2008.9610	2008.9730	2008.9956	2016.5027	2016.5127
2016.5491	2016.5857	2016.6265	2016.6595	2016.6958	2016.6987	2016.7072	2016.7340	2016.7751
2016.7825	2016.7858	2016.8082	2016.8505	2016.8873	2016.9349	2016.9629	2017.0065	2017.0419
2017.0806	2017.1193	2017.1577	2017.2038	2017.2325	2017.2552	2017.2629	2017.2686	2017.2754
2017.2912	2017.3041	2017.3285	2017.3590	2017.3663	2017.3784	2017.4050	2017.4161	2017.4202
2017.4338	2017.4427	2017.4556	2017.4746	2017.5013	2017.5182	2017.5408	2017.5488	2017.5817
2017.5895	2017.6084	2017.6221	2017.6597	2017.6660	2017.6880	2017.6913	2017.7308	2017.7374
2017.7540	2017.7732	2017.8035	2017.8120	2017.8354	2017.8495	2017.9021	2017.9242	2017.9751
2017.9991	2018.0133	2018.0201	2018.0499	2018.0768	2018.0832	2018.0959	2018.1265	2018.1756
2018.1980	2018.2396	2018.2676	2018.2952	2018.2993	2018.3159	2018.3411	2018.3882	2018.4122
2018.4589	2018.4806	2018.5018	2018.5227	2018.5258	2018.5621	2018.5864	2018.5951	2018.6005
2018.6089	2018.6138	2018.6382	2018.6488	2018.6606	2018.6919	2018.7096	2018.7229	2018.7264
2018.7354	2018.7537	2018.7653	2018.7826	2018.8035	2018.8168	2018.8332	2018.8364	2018.8422
2018.8560	2018.9162	2018.9318	2018.9921					

Table 3 Crossing time of the isolated HCS

2007.0220	2007.0701	2007.0972	2007.1433	2007.1536	2007.1699	2007.2189	2007.3169	2007.3793
2007.3911	2007.4327	2007.5248	2007.5453	2007.6652	2007.7418	2007.7758	2007.8530	2007.8862
2007.9249	2007.9822	2007.9957	2007.9991	2008.0309	2008.1827	2008.2543	2008.3298	2008.3807
2008.4434	2008.5067	2008.5521	2008.5773	2008.6256	2008.6480	2008.7240	2008.7740	2008.7946
2008.9610	2016.5127	2016.6265	2016.6595	2016.7072	2016.7340	2016.7751	2016.8082	2016.8505
2016.8873	2016.9629	2017.0065	2017.1193	2017.1577	2017.3285	2017.3663	2017.3784	2017.4050
2017.4338	2017.4746	2017.5013	2017.5408	2017.5488	2017.5817	2017.6221	2017.6597	2017.7308
2017.7540	2017.7732	2017.8035	2017.8354	2017.9021	2017.9751	2018.0133	2018.0499	2018.0768
2018.2396	2018.2676	2018.3159	2018.5018	2018.5864	2018.5951	2018.6005	2018.6382	2018.6606
2018.7096	2018.7354	2018.7537	2018.8168	2018.9162				

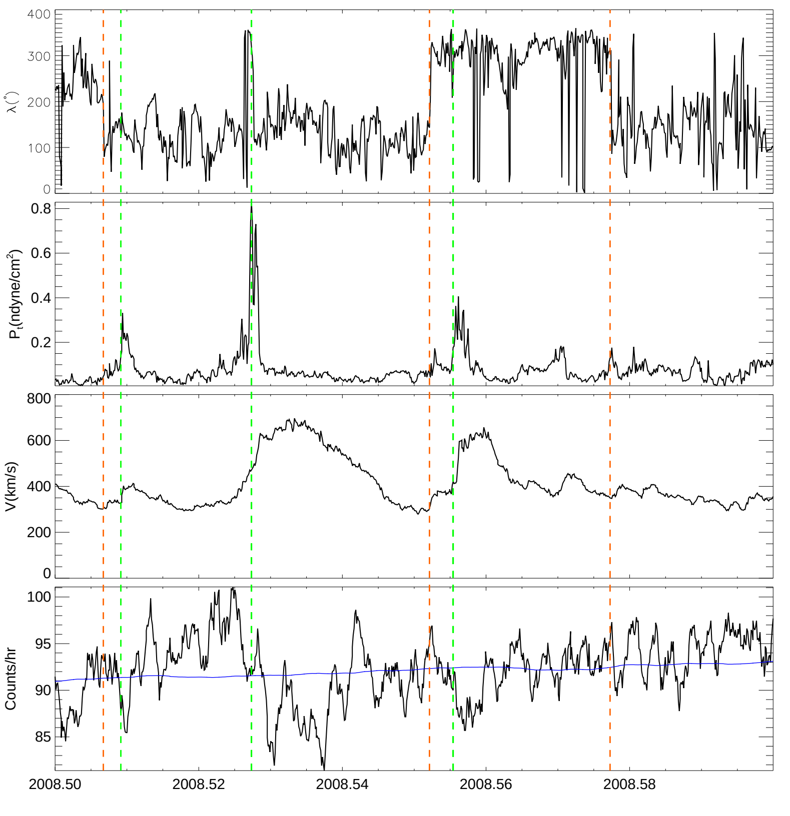

Fig. 1 The temporal variation of the solar wind and GCRs from 2008.5 to 2008.6 (from top to bottom: RTN magnetic longitude, total pressure, flow speed of solar wind, GCR counts). The red and green dashed lines indicate the crossings of HCS and SIs, respectively.

In order to investigate the roles of SI and HCS for the GCR variation, the solar wind events shown in Table 1-2 need to be analyzed statistically. Here we use the Superposed epoch analysis (SEA) method for the SI and HCS crossing events during the two intervals. The zero epoch is set to at the time of the SI or HCS crossing, with a total duration of 8 days. Then all the relevant events are added, and then divided by the number of events. This treatment will remove some random noises, and the physical result is expected to be extracted. The long-term variation of GCR counts (blue curve in Figure 1) will be subtracted from the short-term variation, and then the result is divided by the the long-term variation counts. Finally, the variation rates of the GCR counts are obtained, through which the relation between GCR counts and SIs or HCS will be discussed, as presented in the next section.

3. STATISTICAL RESULTS

First, the SEA method is used for the SI events listed in Table 1, which are grouped as catalogue 1. Figure 2 shows the solar wind and GCR variations near SIs, including the solar wind speed, estimated radial and azimuthal components of diffusion coefficients (κ_{rr} and $\kappa_{\phi\phi}$) of GCRs, magnetic field strength, and GCR counts. The black and blue curves correspond to the profiles for the two intervals, respectively. The vertical dashed red line marks the epoch time of SI, across which the solar wind speed increases from ~ 350 km/s to ~ 540 km/s. The solar wind is highly compressed at SI with a peak of magnetic field strength, which is two times of those in the slow and fast solar wind. From the Quasi-linear theory (QLT), the parallel diffusion along magnetic field is inversely proportional to the magnetic turbulence strength $\langle \delta B^2 \rangle / B^2$[30], where $\langle \delta B^2 \rangle$ is the mean square of the magnetic turbulence, and B the mean magnetic field strength. The diffusion perpendicular to magnetic field is more complicated and less understood, generally treated as positively correlated with the turbulence strength[31]. Based on the turbulence theories, the diffusion coefficients near SIs during the recent two solar minimums were calculated in the recent work[19]. Here we follow a different approach based on an empirical expression to estimate the parallel diffusion along the magnetic field[32]

$$\kappa_{\parallel} = \kappa_{\parallel 0} \beta \frac{B_n}{B_m} \left(\frac{P}{P_0} \right)^a \left[\frac{\left(\frac{P}{P_0} \right)^c + (\frac{P_k}{P_0})^c}{1 + (\frac{P_k}{P_0})^c} \right]^{\left(\frac{b-a}{c} \right)} , \tag{1}$$

here $\kappa_{\parallel 0}$ is a constant, and set to $3.0 \times 10^{22} cm^2/s$, $\beta = v/c$ is the ratio of particle speed to light speed, $P_0 = 1$ GV is the reference rigidity, P_k the particle rigidity, B_m the magnitude of interplanetary magnetic field, $B_n = 1$ nT the reference magnetic field; a and b are the preset coefficients that indicate the dependence slope between diffusion coefficient and rigidity, and c gives the smoothness between the two slopes. Here we choose $a = 0.4$, $b = 1.95$, and $c = 3.0$, upon which the calculated diffusion coefficients are successfully used to fit the observed global variation of GCRs during the last solar minimum (2006-2009). Using the above parameters, the obtained parallel diffusion coefficient of 100 MV protons is $\sim 1.26 \times 10^{21} cm^2/s$, and agrees with the estimation based on theory and observation[33,34]. For the perpendicular diffusion, instead of the turbulence-dependent diffusion model, e.g., the non-linear guiding center (NLGC) model[31], here we use a simple expression $\kappa_\perp = 0.02\kappa_\parallel$, in which the two component diffusions are positively correlated, and no turbulence is taken into account. In a heliocentric spherical coordinate system (r, θ, ϕ), the radial and azimuthal components of the diffusion coefficients are respectively written as[35]

$$\kappa_{rr} = \kappa_\parallel \cos^2\psi + \kappa_{\perp r} \sin^2\psi \,, \tag{2}$$

$$\kappa_{\phi\phi} = \kappa_\parallel \sin^2\psi + \kappa_{\perp r} \cos^2\psi \,, \tag{3}$$

here ψ is the spiral angle measuring the deviation of the heliospheric magnetic field to the radial direction. Because $\psi \sim 45°$ at the heliocentric distance of 1 AU, the radial and azimuthal components of the diffusion coefficients are similar, $\kappa_{rr} \simeq \kappa_{\phi\phi}$. Taking an Oxygen ion with energy of 300 MeV·nuc^{-1} for one example, the calculated component diffusion coefficients near SIs are shown in the panel B of Figure 2.

The diffusion coefficient for interval 1 is larger than that of interval 2 because the former magnetic field is weaker than the latter shown in the panel C of Figure 2. At the point of SI crossing, both diffusion coefficients drop to a low value of $\sim 1.4 \times 10^{21} cm^2/s$, about 1/3 of those before the crossing. The corresponding GCR variation rates drop dramatically near the SI, from $\sim 1\%$ to $\sim -0.7\%$. Note that the GCR count rates are different for the two intervals. For interval 1, the GCR count rate begins to increase two days prior to the crossing, and reaches the maximum at the time of ~ -1 day. After that, it decreases to the bottom about half a day after the crossing, and stays at a low count rate of $\sim -1\%$ for the next several days. The temporal enhancement of GCR counts before SI crossing acts as a barrier to GCR propagation, and is known as the so-called "snow-plough" effect, which was also mentioned in the previous literature[22]. For interval 2, the GCR count rate varies differently, and keeps nearly constant $\sim 1\%$ until ~ 1 day before SI, after that it begins to drop and reaches the bottom of $\sim -1\%$ at ~ 1.5 day after the SI, and recovers steadily to the rate $\sim 1\%$ at the end. Obviously, no "snow-plough" effect appears for interval 2. This different behavior of GCR variation for SI crossing is believed to be associated with the different physical mechanisms during the two intervals. The previous research indicated that the lower-energy (e.g., < 1 GeV·nuc^{-1}) GCR intensities were lower at low latitude during interval 1 ($qA < 0$) than interval 2 ($qA > 0$)[6]. As the panel B of Figure 2 shows, the "snow-plough" effect during interval 1 may be interpreted as the sudden drop of the radial diffusion coefficient (κ_{rr}) near SIs, which results in the inefficient inward transport of GCRs along the radial direction, and the GCRs accumulate ahead of SIs. As for interval 2, we argue that the diffusion coefficients shown as the blue curve in the panel B of Figure 2 may not be accurate because the following two factors: first, the free parameters chosen in the above diffusion expression were only valid for interval 1; second, the obtained diffusion coefficients for interval 2 predict the presence of "snow-plough" before SIs, which differs from the observed depletion of GCR counts roughly from day 0 to 2 near SIs. These indicate that the effective GCR transport becomes much faster in the regions of fast solar wind than the slow solar wind for interval 2, which is opposite to that for interval 1. Being similar to SIs, the heliopause is ideally treated as a tangential discontinuity as well, beyond which the anomalous cosmic rays (ACRs) were found to escape rapidly when entering the interstellar space[36,37]. The reason is that the diffusion coefficients of cosmic rays are extremely large above the heliopause due to the local none-scattering magnetic environment. Further efforts are needed for a more efficient model of transport coefficients in order to explain this phenomenon.

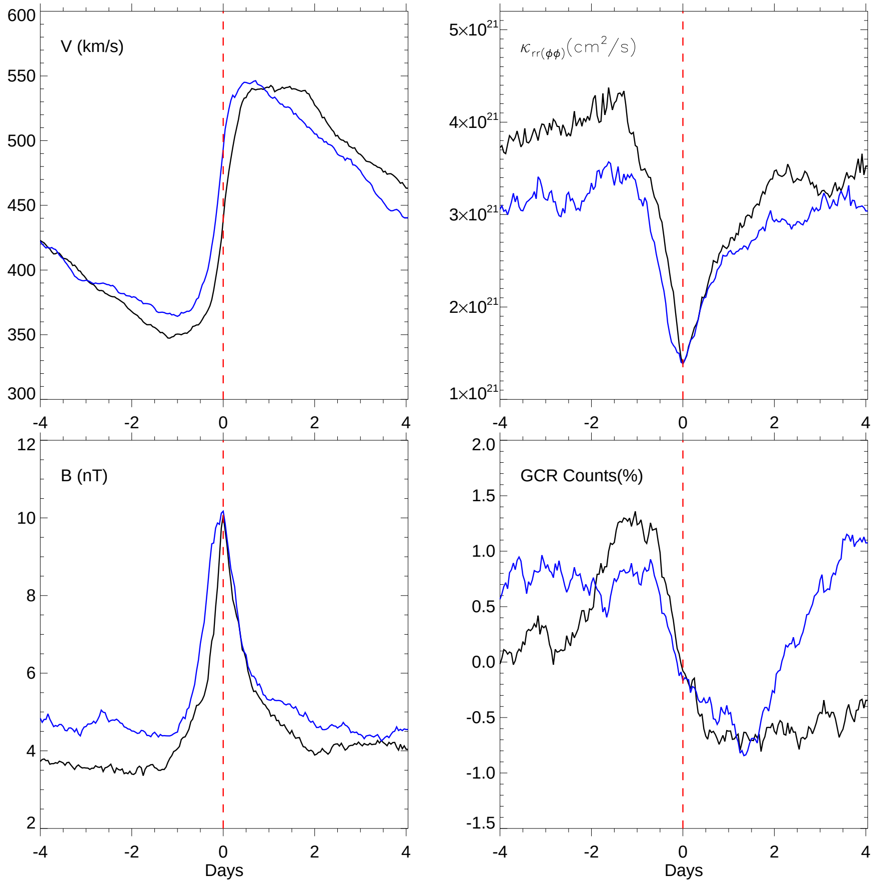

Fig. 2 The SEA results for SI crossings for the two intervals, showing (A) solar wind speed, (B) radial and azimuthal components of diffusion coefficients, (C) magnetic field strength, and (D) the GCR count rates. The black and blue curves correspond to interval 1 and 2, respectively. The vertical dashed lines show the zero epoch time of SI crossing. The dotted-dashed orange curves show the Monte-Carlo means, and the upper and lower dotted orange curves correspond to 5% and 95% confidence level of the variations.

Next the correlation between GCR count rate and all the HCS is investigated through the SEA method, the HCS crossing events are listed in Table 2. Figure 3 shows the corresponding variations of solar wind speed, component diffusion coefficients, magnetic field strength, and GCR variation near HCS. The vertical red dashed lines mark the zero epoch of HCS crossing. During solar minimum, HCS is closely associated with slow solar wind that originates from low latitude region on solar surface[38]. In practice, some HCS locate very near to SIs, and the solar wind speed has an apparent increase after the HCS crossing, which indicates that the effect of HCS on GCRs can not correctly be evaluated because of the influence of the adjacent SIs. After the HCS crossing, not only the azimuthal angle changes nearly oppositely but also the magnitude has an abrupt enhancement for the magnetic field.

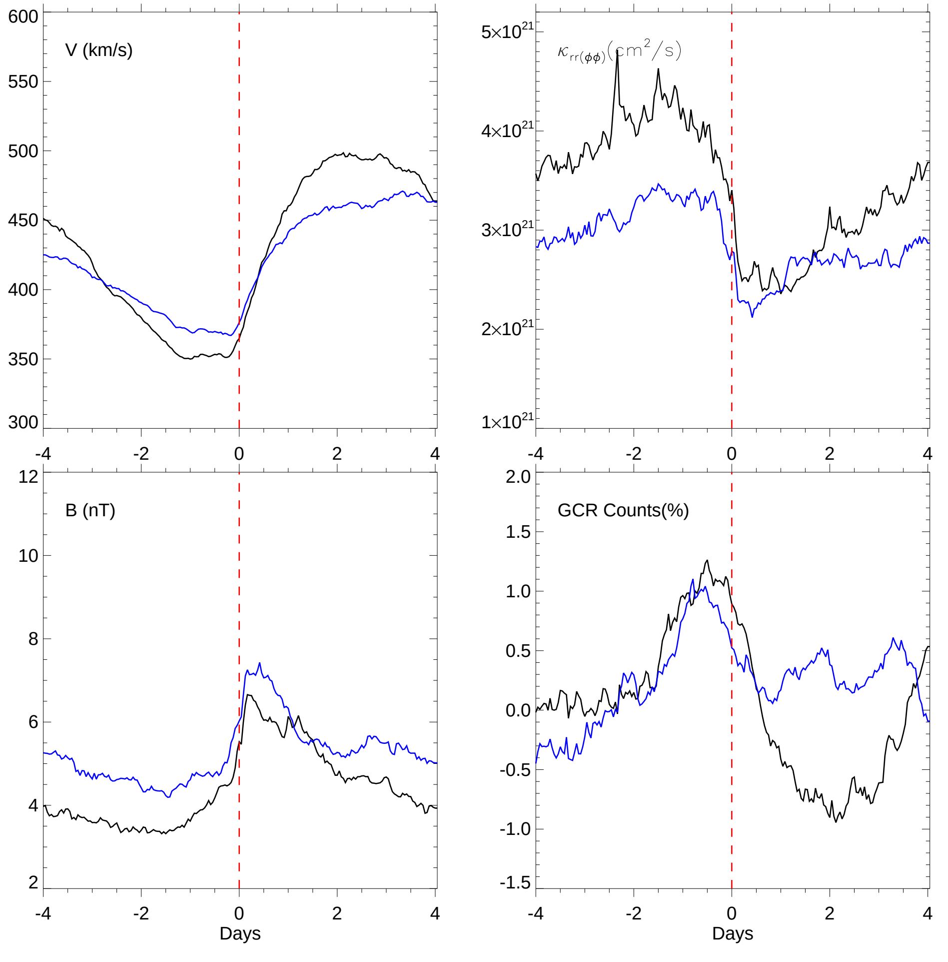

Fig. 3 Similar to Figure 2, the SEA results near all the currents.

The HCS mainly resides in the low speed solar wind, with around 1.5 times enhancement for the magnetic field strength after the HCS crossing. As a result, the component diffusion coefficients decline simultaneously near HCS for the two intervals, especially for interval 1 when the diffusion coefficients reduce nearly in half after the crossing. As the panel D of Figure 3 shows, the GCR count rates are expected to decrease as well. The GCRs accumulate and form the "snow-plough" shape, with a peak at ~ -1 day before the crossing. This is similar to the phenomenon for interval 1 shown in Figure 2, while the peak of GCR count rate appears much closer to the HCS crossing for the current case, showing the dominance of drift effects of HCS on the GCR accumulation. After that, the GCRs drop to a much lower value for interval 1 than interval 2, as predicted from the different changes of diffusion coefficients near HCS. In these cases, we may conclude that the GCR variation is caused by a combined effect of the diffusion near SIs and the drift near HCS.

In order to evaluate the effects of isolated HCS on GCR variation, it is necessary to remove the events of current sheets near SIs, and those that locate closely with each other. Based Table 1 and 2, the current sheets that are within around one day of the adjacent SIs are excluded. The filtered events are presented in Table 3. Figure 4 shows the corresponding SEA results. There is no sharp jump for the solar wind speed because the current sheets near SIs are all excluded. The HCS locates in the valley of slow solar wind profile as predicted, which indicates that most of the obtained HCS originates from the low latitude solar surface. The magnetic field strength for interval 1 is smaller than that for interval 2, they all vary with a slightly increasing tendency, and no shear or compressed flows exist near the HCS. Compared with the previous plots, the component diffusion coefficients decrease much gradually after the HCS crossing, indicating that the diffusion effect is less important than the previous cases. The GCR counts have a peak that centers around the HCS, and declines with a distance away from the zero epoch. Being consistent with the theory[39] and observation[40], this result shows that the GCRs accumulate near the HCS through the drift mechanism, and decrease at the two sides of the HCS as they diffuse away from the HCS. Different from the previous work[22], the polarities of the HCS depend on the radial component of magnetic field in northern heliosphere, the Away-Toward and Toward-Away are not discussed in this work. Here we only focus on the combined effects of HCS on the GCR variation during the solar minimums.

From above, the different roles of SIs and HCS on GCRs variation are presented from the SEA analysis based on the three tables. In summary, the SI crossings inside CIRs lead to the significant changes of diffusion coefficient, and the subsequent drop of GCR counts. For interval 1, the "snow-plough" of GCR counts may be caused by the sudden drop of radial diffusion coefficient at SIs; however, the depletion of GCR counts after SI crossing for interval 2 may correlate with the escape of GCR particles in the fast solar wind, which may correspond to a sudden increase of radial diffusion coefficient from the theory. The HCS is an important factor that causes the accumulation of GCR counts around it through drift mechanism.

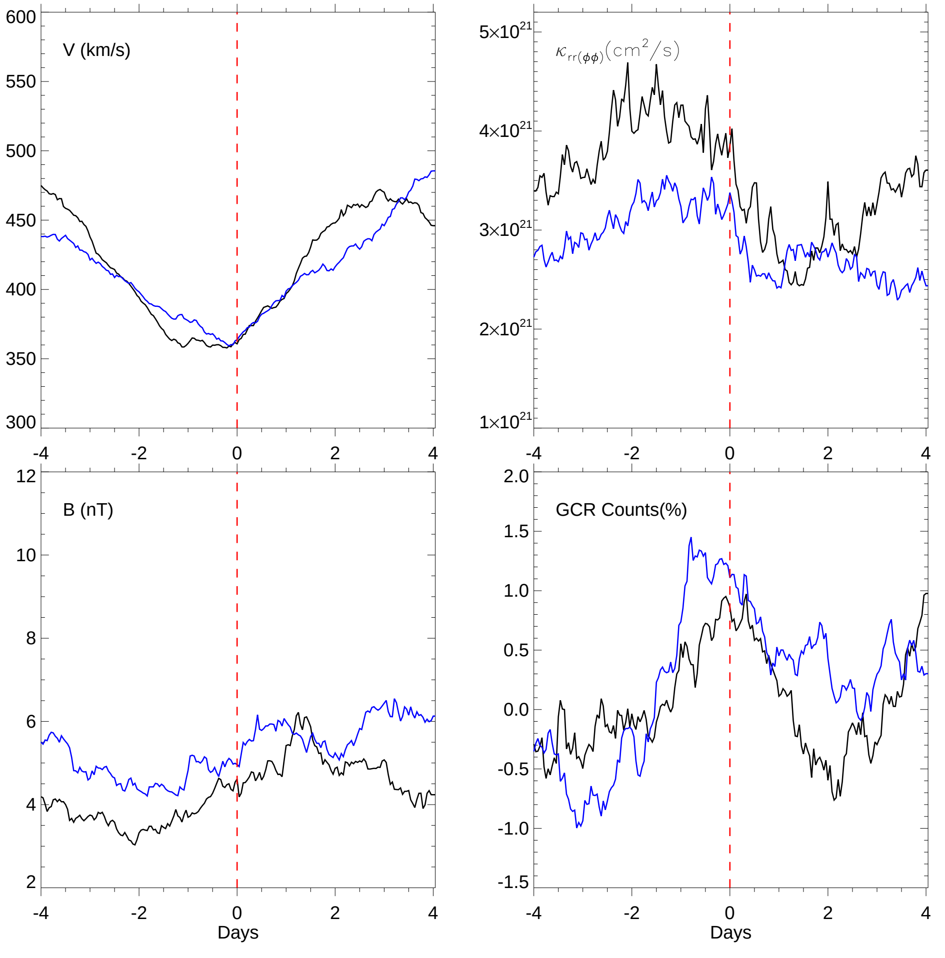

Fig. 4 Similar to Figure 3, the SEA results near the individual HCS.

4. DISCUSSIONS

The physics of GCR variation in solar wind can be presented using the Parker transport equation written as[5]

$$\frac{\partial f}{\partial t} + (\mathbf{u} + \mathbf{v}_d)\nabla f - \nabla \cdot (\boldsymbol{\kappa} \cdot \nabla f) - \frac{\nabla \cdot \mathbf{u}}{3} \frac{\partial f}{\partial \ln p} = 0 \,. \tag{4}$$

Here $f(\mathbf{r}, p)$ is the isotropic cosmic ray distribution in phase space as a function of spatial position $\mathbf{r}$ and the magnitude of momentum p, $\mathbf{u}$ is the solar wind velocity, $\boldsymbol{\kappa}$ is the diffusion tensor, and $\mathbf{v}_d$ is the drift velocity that includes the gradient and curvature drifts for an isotropic distribution of particles. After ignoring the adiabatic energy term, the GCR distribution is mainly related to the combined effect of the three factors: the convection speed $\mathbf{u}$, the drift speed $\mathbf{v}_d$, and the diffusion speed $\nabla \cdot \boldsymbol{\kappa}$. The largest one determines the main mechanism among the above three speeds. The diffusion speed $(\nabla \cdot \boldsymbol{\kappa})_r \sim \kappa_{rr}/r$ in the solar wind, and r is the heliocentric distance from the Sun center. Given $\kappa_{rr} = 3.0 \times 10^{21}\ cm^2/s$, the diffusion speed is $\sim$ 2000 km/s at regions of $r = 1$ AU, which is much larger than the solar wind speed $\sim$ 350–550 km/s. This result is consistent with the previous calculation based on observation[19] and simulation[18]. Although it was shown that the GCR counts are often found to correlate with solar wind speed well at 1 AU[16], and the modulation parameter of GCRs was proportional to the product of solar wind speed and magnetic field strength, the theoretical analysis indicated this phenomenon is directly caused by the diffusion coefficients[3], thus the convection effect is not important compared to the diffusion.

In a weak turbulent solar wind, the drift velocity is approximated as $\mathbf{v}_d = \frac{pv}{3q} \nabla \times (\frac{\mathbf{B}}{B^2})$, where v is the particle speed, q is the particle charge, and B the magnetic field. Here we can not estimate the drift speed from the single-point observation. Based on a simplified HCS model in which the magnetic field strength does not change across HCS, the previous simulation work indicated that the drift effect is less important than the diffusion at 1 AU[18], the GCRs can not accumulate near the HCS, and it seems that the HCS does not organize the GCR variation. In the reality, the geometry of HCS is much more complicated than the model (see Figure 1), not only the direction but also the strength of the magnetic field changes across HCS, the drift effect may have been underestimated as we mentioned in the literature. From Figure 4, it is apparent that the GCRs accumulate near individual HCS for the two intervals, indicating that the drift effect dominates over the diffusion. In this work, although the energy range of GCRs is 100–500 MeV$\cdot$nuc^{-1} and much smaller than that of the neutron monitors on ground (beyond several GeV$\cdot$nuc^{-1}), the SEA results are similar to the previous investigation which was based on the neutron monitors[22]. Since the convection effects are much smaller than the diffusion, we may conclude that during the past two solar minimum periods, the importance of drift, diffusion, and convection declines for GCR transport at 1 AU.

5. CONCLUSIONS

In this work, we have studied the variation of GCRs and solar wind during the two solar minimum periods, 2007.0-2009.0 and 2016.5-2019.0, based on ACE observation. The relation between GCR counts and the two typical solar wind structures, SIs and HCS, was investigated based on the SEA method. The data were grouped into the three categories, the crossing time of SIs, all HCS, and isolated HCS. For interval 1, the GCR counts formed the “snow-plough” effect before the SIs, after that GCRs dropped substantially. This phenomenon was believed to be associated with the sudden drop of diffusion coefficients near SIs. For interval 2, no “snow-plough” effect was found, and the GCRs kept nearly constant before SIs, then dropped rapidly after SI crossing, and recovered in several days; this result indicated that the GCRs escape after entering the region of fast solar wind, where the diffusion coefficients should be higher than that in slow solar wind.

The GCRs were found to be peak near HCS for the two intervals, showing that the HCS was an important channel for the transport, and the associated drift effect was dominant. Based on the theoretical analysis, we may conclude that during the solar minimum, the dominance of drift, diffusion, and convection effects on the GCRs decreases successively at 1 AU. The diffusion plays the most important role on the GCR variation near SIs, and the combined effects of diffusion and drift determine the GCR counts near HCS.

References

1 Ackermann, M., et al., Science, 2013, 339, 6424, 807

2 Cummings A. C. Stone E. C., Heikkila B. C., et al., ApJ, 2016, 831, 18

3 Jokipii J. R., in The Outer Heliosphere, The Next Frontiers, Edited by Scherer K. H., Fichtner H. J., Fahr and Marsch E., COSPAR Coll. Ser., 11. Amsterdam, Pergamon Press, 513–519

4 Schlickeiser R., Cosmic Ray Astrophysics (Berlin, Springer), 2002

5 Parker E. N., Planet. Space Sci, 1965, 13, 9

6 Jokipii J. R., & Kopriva D. A., ApJ, 1979, 234, 384

7 Kota J., & Jokipii J. R., Geophys. Res. Lett, 1991, 18, 1979

8 Jokipii J. R., & Thomas B., ApJ, 1981, 243, 1115

9 Alania M. V., Modzelewska R., & Wawrzynczak A., Sol. Phys, 2011, 270, 629

10 Burlaga L. F., McDonald F. B., Ness N. F., et al., J. Geophys. Res, 1984, 89, 6579

11 Potgieter M. S., & Le Roux J. A., ApJ, 1994, 423, 817

12 Langner U. W., & Potgieter M. S., Ann. Geophys, 2004, 22, 3063

13 Sarabhai V., J. Geophys. Res, 1963, 68, 1555

14 Siscoe G. L., J. Geophys. Res, 1972, 77, 27

15 Richardson I. G., Space Sci. Rev, 2004, 111, 267

16 Leske R. A., Cummings A. C., Mewaldt R. A., Stone E. C., SSRv, 2013, 176, 253

17 Richardson I. G., J. Geophys. Res, 1996, 101, 13483

18 Guo X., & Florinski V., ApJ, 2016, 826, 65

19 Ghanbari K., Florinski V., Guo X., et al., ApJ, 2019, 882, 54

20 Badruddin R. S. Yadav, & Vadav N. R., Planet. Space Sci, 1985, 33, 191

21 El Borie M. A., J. Phys. G., 2001, 27, 773

22 Thomas S. R., Owens M. J., Lockwood M., & Scott C. J., Solar Phys, 2014, 289, 2653

23 Okazaki Y., Fushishita A., Narumi T., Kato C., et al., ApJ, 2008, 681, 693

24 Stone E. C., Frandsen A. M., Mewaldt R. A., et al., SSRv, 1998, 86, 1

25 Abramenko V., Yurchyshyn V., Linker J., et al., ApJ, 2010, 712, 813

26 McComas D. J., Ebert R. W., Elliott H. A., et al., Geophys. Res. Lett, 2008, 35, L18103

27 Jian L., Russell C. T., Luhmann J. G., Skoug R. M., Sol. Phys, 2006, 239, 337

28 Jian L., Russell C. T., Luhmann J. G., Sol. Phys, 2011, 274, 321

29 Jian L. K., MacNeice P. J., Taktakishvili A., et al., Space Weather, 2015, 13, 316

30 Giacalone J., & Jokipii J. R., ApJ, 1999, 520, 204

31 Matthaeus W. H., Qin G., Bieber J. W., Zank G. P., ApJ, 2003, 590, L53

32 Potgieter M. S., Sol. Phys, 2013, 10, 3

33 Potgieter M. S., Vos E. E., Boezio M., et al., Sol. Phys, 2014, 289, 391

34 Giacalone J., SSRv, 1998, 83, 351

35 Potgieter M. S., Living Rev. Solar Phys, 2013, 10, 3

36 Stone E. C., Cummings A. C., McDonald F. B., et al., Science, 2013, 341 150

37 Florinski V., Jokipii J. R., Alouani-bibi F., et al., ApJ, 2013, 776, L37

38 Smith E. J., J. Geophys. Res, 2000, 106, 15, 819

39 Kota J. & Jokipii J. R., ApJ, 1983, 265, 573

40 Newkirk G., & Lockwood J. A., Geophys. Res. Lett, 1981, 8, 619